







Membrane III-V/Si DFB Laser Using Uniform Grating and Width-Modulated Si Waveguide

Takuma Aihara , Member, IEEE, Tatsuro Hiraki , Member, IEEE, Takuro Fujii , Member, IEEE, Koji Takeda , Senior Member, IEEE, Takaaki Kakitsuka , Member, IEEE, Tai Tsuchizawa, and Shinji Matsuo , Fellow, IEEE

Abstract—Membrane buried-heterostructure III-V/Si distributed feedback (DFB) lasers with a stopband-modulated cavity on a Si substrate have been developed. The membrane III-V layers with 230-nm thickness enable us to construct an optical supermode with a 220-nm-thick Si waveguide that is used in standard Si photonics platform. We employ a uniform grating and Si waveguide, in which Si waveguide width is modulated to control the center wavelength of the stopband. The cavity can be designed by controlling the modulation width and modulation length of Si waveguide. Therefore, it is easy to engineer and fabricate the laser cavity compared with the cavity using $\lambda/4$ -phase shift grating. Output light from the cavity is coupled to Si waveguide through InP inverse taper waveguide, and then coupled to SiO_x waveguide through Si inverse taper waveguide, which provides the 2-dB fiber coupling loss. We have demonstrated single-mode lasing by using Si waveguide, where its width is increased 80 nm at the center of the cavity. The threshold current and maximum fiber output power are 3 mA and 4 mW, respectively. By extending the active region length to 1 mm, 17-mW fiber coupled output power is obtained. High-temperature operation up to 130 °C is also obtained with a 1-mW fiber output power.

Index Terms—Photonic integrated circuits, semiconductor lasers, silicon photonics.

I. INTRODUCTION

WITH the rapid increase in network traffic, more and more high-capacity optical transmitters are required. A Mach-Zehnder modulator (MZM) integrated with a narrow-linewidth laser is a candidate for high-capacity optical transmitters because it provides high-throughput by using both amplitude and phase modulations [1]. A polarization rotator, splitter/combiner, and optical wavelength multiplexer are also essential elements to increase the data capacity by the polarization and wavelength multiplexing [2], [3]. Moreover, large-scale photonic integrated

circuits (PICs) on Si photonics platforms would enable many components to be integrated at a low cost [4]. This is because the assembly costs can be reduced and mature Si complementary metal-oxide-semiconductor (CMOS) manufacturing technology can be employed. Thus, great potential is seen in fabricating PICs on Si substrate including lasers and MZMs for making high-capacity optical transmitters at a low cost. However, there is remaining issue for the wafer-scale integration of lasers on well-developed Si photonics platform since the Si is an indirect-bandgap semiconductor material.

Heterogeneously integrated III-V lasers on Si substrate have been developed by using direct bonding techniques [5]–[15], and the production is now in progress. These lasers use a vertical *p-i-n* junction, in which the total thickness of the III-V layers exceeds 2 μm to ensure a sufficient distance between the optical mode field and contact metals. To control the optical mode between the Si and III-V layers, the effective indices of the Si and III-V layers should be comparable; therefore the optically coupled Si waveguide needs to be as thick as 400–500 nm. On the other hand, well-developed Si devices have been based on 200–300-nm-thick Si waveguides, enabling a small bending radius and efficient optical modulation in MZMs. As a result, the thickness mismatch makes wafer-scale laser integration on Si photonics platforms difficult.

We have proposed to use membrane buried-heterostructure (BH) lasers whose III-V layer thickness is less than 350 nm [16]–[21]. The membrane III-V layer enables us to construct the low-loss optical coupling with a 220-nm-thick Si waveguide because the effective index of membrane III-V layer is comparable with that of the 220-nm-thick Si waveguide. This enables the wafer-scale laser integration on a Si photonics platform without having to change the thickness of the Si waveguide. Indeed, we have developed the distributed feedback (DFB) membrane laser integrated with a Si waveguide on Si platform [21].

For the next step, it is important to narrowing its linewidth and increasing output power. Recently, narrow-linewidth lasers on Si substrate have been developed, in which the low-loss Si waveguide is used for increasing the cavity Q factor [12]–[15]. In addition, heterogeneously integrated DFB lasers, in which a 500-nm thick Si waveguide is optically coupled with an active III-V layer, exhibited ultra-narrow linewidth of 18 kHz [7], [8]. In these DFB lasers, an optical confinement factor in the low-loss Si waveguide is much larger than that of the lossy III-V layer, which can be reduced the modal loss in the cavity. High-Q cavities are also achieved by using the stopband modulation

Manuscript received November 15, 2019; revised February 13, 2020; accepted February 23, 2020. Date of publication March 9, 2020; date of current version May 27, 2020. (Corresponding author: Takuma Aihara.)

Takuma Aihara, Tatsuro Hiraki, Takuro Fujii, Koji Takeda, Tai Tsuchizawa, and Shinji Matsuo are with NTT Device Technology Labs, NTT Corporation, Atsugi 243-0198, Japan (e-mail: takuma.aihara.vp@hco.ntt.co.jp; tatsuro.hiraki.gu@hco.ntt.co.jp; takuro.fujii.uc@hco.ntt.co.jp; koji.takeda.vk@hco.ntt.co.jp; tai.tsuchizawa.ya@hco.ntt.co.jp; shinji.matsuo.vk@hco.ntt.co.jp).

Takaaki Kakitsuka was with NTT Device Technology Labs, NTT Corporation, Atsugi 243-0198, Japan. He is now with Graduate School of Information, Production and Systems, Waseda University, Fukuoka 808-0135, Japan (e-mail: t.kakitsuka@waseda.jp).

Color versions of one or more of the figures in this article are available online at <http://ieeexplore.ieee.org>.

Digital Object Identifier 10.1109/JLT.2020.2978808

[22]–[25]. In addition, stopband modulation can reduce the peak intensity inside the cavity, which is similar to the strategy shown in [26]–[28]. Thanks to low optical confinement factor in active region and the reduction of peak intensity inside the cavity, spatial-hole burning is suppressed even in high-Q cavity laser. In ref. [7], the grating is formed on the Si waveguide by etching the apertures with uniform pitch and locally modulated width to construct the stopband-modulated cavity. However, we seem that fabricating the grating has some difficulties as follows. Since optical mode is mainly confined in Si waveguide and the low coupling coefficient is necessary for long-cavity DFB lasers [29], gratings with shallow and small aperture are required on the Si waveguide, which are sensitive to the grating characteristics.

In this work, we have proposed the membrane BH DFB laser using an optically coupled III-V/Si waveguide, in which we use uniform SiN grating on top-surface of InP layer and width-modulated stripe Si waveguide [30]. The fabrication of the SiN grating is tolerant because its depth is determined by the uniformity of deposition and highly selective etching between SiN and InP is available. In addition, width modulation in 220-nm thick stripe Si waveguide is easily achieved by using conventional photolithography. In this paper, we have demonstrated the single-mode lasing by using the uniform surface SiN grating and width-modulated Si waveguide. For 500- μm long DFB laser, the threshold current and the maximum fiber output power of are 3 mA and 4 mW, respectively. The Lorentzian linewidth is estimated to be about 300 kHz when the bias current of 54 mA. By extending the active region length to 1 mm, 17-mW fiber coupled output power is obtained. The high-temperature operation up to 130 $^{\circ}\text{C}$ is also obtained.

Section II describes the device structure and operating principle of the cavity with stopband modulation. Section III describes the fabrication procedure of the laser. Section IV describes the experimental results on the fabricated laser. Section V is the conclusion.

II. OPERATING PRINCIPLE

A. Device Structure

Fig. 1(a) shows a cross-sectional view of a membrane BH DFB laser using the optically coupled III-V/Si waveguide. The III-V layer consists of an InGaAsP-based multiple quantum well (MQW) core region buried in a membrane InP layer, and it has a lateral *p-i-n* junction. The optical absorption in the contact materials can be neglected when the optical mode field is far enough away from the contact materials. The current is injected into the buried MQW from the lateral direction. This lateral current injection structure enables us to reduce the total thickness of the III-V layer, which results in a reduction of its effective index. Since the effective indices of Si and III-V layers are comparable, an optical supermode between the membrane III-V layer and a 220-nm-thick Si waveguide can be constructed. A uniform SiN grating is formed on the top-surface of the III-V layer.

Fig. 1(b) shows a top view of schematic diagram of Si waveguide underneath the III-V layer. The Si waveguide becomes wider at the middle of the cavity. Since the effective refractive index of the III-V/Si waveguide increases with increasing the Si

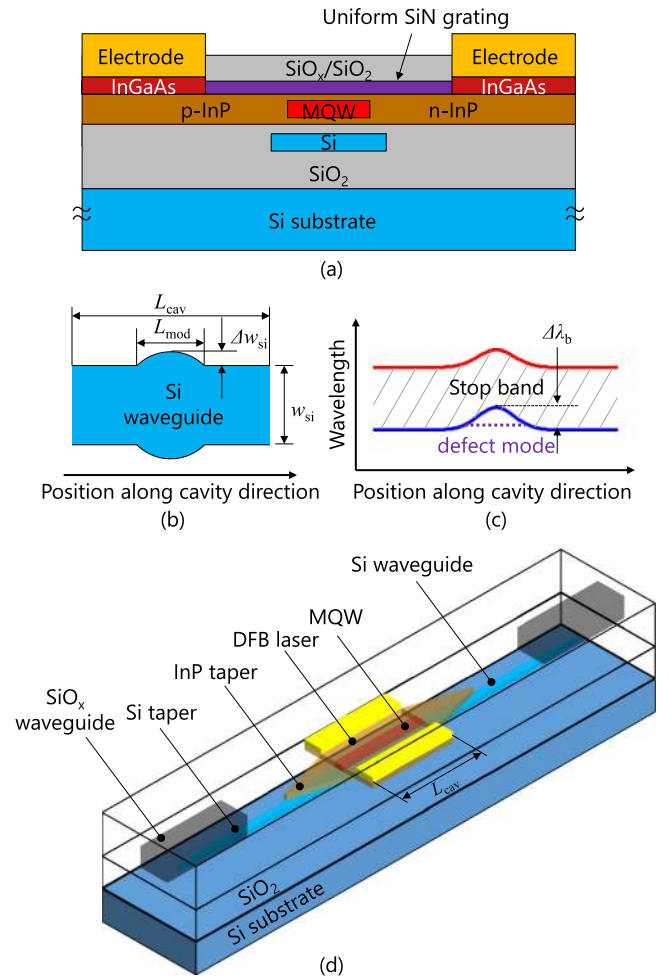


Fig. 1. (a) Cross-sectional view of membrane BH DFB laser using optically coupled III-V/Si waveguide. (b) Top view of Si waveguide underneath III-V layer. (c) Schematic diagram of stopband with its modulation. (d) Bird's eye view of device including DFB laser, Si waveguide, and SiO_x waveguide.

waveguide width, the stopband of the cavity shifts to a longer wavelength, as schematically illustrated in Fig. 1(c). As shown, the stopband modulation creates a defect mode in the cavity. The threshold gain for the defect mode can be controlled by the stopband modulation profile described below. When the threshold gain for the fundamental defect mode is designed to be lower than those of other modes, single-mode lasing for the defect mode is achieved.

The light emitted from the DFB laser is coupled to the Si waveguide through the InP inverse taper waveguide as shown in Fig. 1(d). This optical mode transfer is easily achieved because of their comparable effective indices. The SiO_x waveguides are also used for efficient fiber coupling, where the Si inverse taper waveguide are used to reduce the optical loss at the spot-size convertor.

B. Design of Optical Confinement

First, we show the calculated filling factors in p-type InP, $\Gamma_{\text{p-InP}}$, MQWs, Γ_{MQWs} , SiN, Γ_{SiN} , and Si, Γ_{Si} , depending on the Si waveguide width w_{Si} . Since absorption loss in p-InP layer is

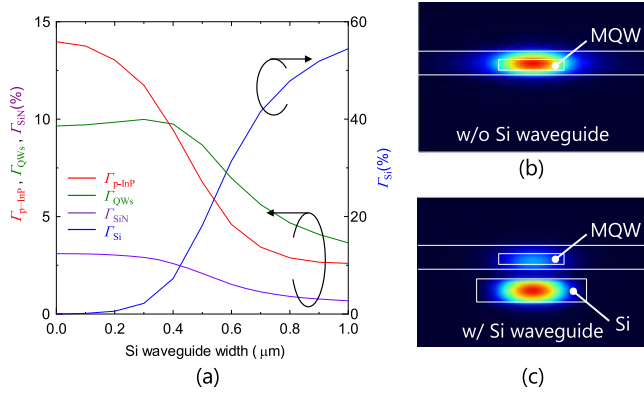


Fig. 2. (a) Calculated filling factors in p-InP, MQWs, and Si depending on Si waveguide width. Calculated optical intensity distribution of waveguide without (b) and with Si (c).

dominant, it is important to reduce $\Gamma_{p\text{-InP}}$. As shown in Fig. 2(a), $\Gamma_{p\text{-InP}}$ dramatically decreases with increasing w_{Si} up to 0.8 μm above which it becomes almost constant. As can be seen in Fig. 2(b), the optical mode field is mainly confined in the MQW core when there is no Si waveguide. On the other hand, by using the 1- μm -wide Si waveguide, the optical field is mainly confined in the Si waveguide, while the optical field is still confined in the MQWs for ensuring the optical gain, as shown in Fig. 2(c). These results indicate that the optical mode field can be controlled by changing the width of the Si waveguide. We designed the Si waveguide width to be wider than 0.8 μm to reduce the modal loss in the cavity.

C. Design of Stopband Modulation

We calculated the behavior of the stopband modulation in the cavity by using the transfer matrix model. We used the stopband modulation with a Gaussian function for a smooth refractive index change. Calculated threshold gains are shown in Fig. 3(a) for different modulation depths $\Delta\lambda_b$. In the calculations, the total cavity length L_{cav} and the modulation length L_{mod} were 500 μm and 50 μm , respectively. As shown in Fig. 3(a), both longer and shorter wavelength modes have the same threshold gain when there is no stopband modulation ($\Delta\lambda_b = 0$ nm). When the stopband modulation is to the longer wavelength side ($\Delta\lambda_b = 3$ nm), the threshold gain for the shorter wavelength mode decreases and the threshold gain for the longer wavelength mode increases. This is because a defect mode is created inside the stopband by the modulation on the shorter wavelength side, and the longer wavelength mode is suppressed by the stopband, as shown in Fig. 1(c). By increasing the stopband modulation depth ($\Delta\lambda_b = 6$ nm), the threshold gain for the defect mode still decreases, and the threshold gain for the longer wavelength mode still increases. As a result, the threshold gain difference between the fundamental mode and second mode is increased. When the stopband modulation depth is increased further ($\Delta\lambda_b = 9$ nm), the threshold gain for the second defect mode is also decreased, resulting in a reduction of the threshold gain difference. Fig. 3(b) summarizes the threshold gain for the fundamental mode (g_{th0}) and second mode (g_{th1}) and their difference (Δg_{th}) depending

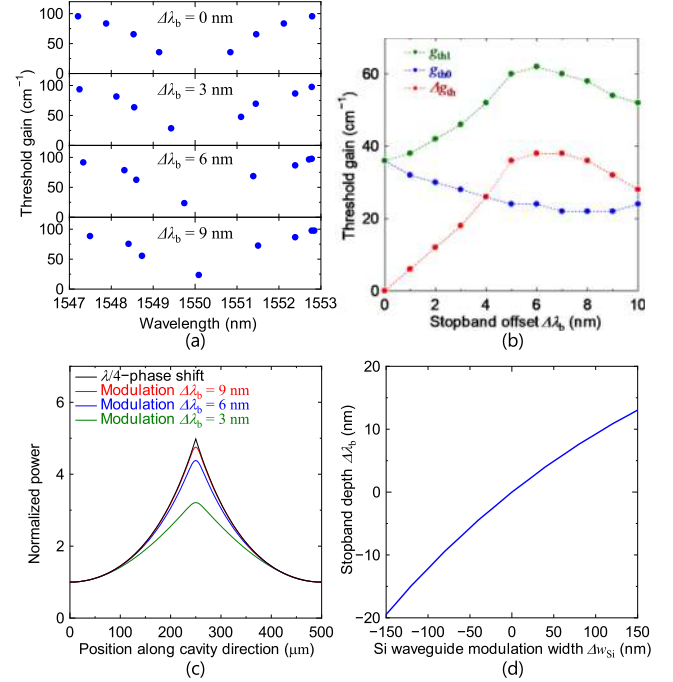


Fig. 3. (a) Calculated threshold gain as a function of wavelength for different modulation depths. (b) Calculated threshold gain for the fundamental mode and second mode, and their difference dependence on modulation depth. (c) Calculated intensity distribution along the cavity direction for different modulation depths. (d) Calculated relationship between stopband modulation depth and Si waveguide modulation width.

on the modulation depth. These results indicate that we can reduce the threshold gain for the fundamental defect mode and maximize the threshold gain difference with the high-order mode by using the stopband modulation.

Fig. 3(c) shows the calculated intensity distribution for the cavity with the stopband modulation for different stopband modulation depths. The intensity distribution in the cavity with a $\lambda/4$ -phase shift is also shown for comparison. The stopband modulation provides smoother and mitigated intensity localization compared with the cavity with the $\lambda/4$ -phase shift.

Next, we calculated the relationship between the depth of the stopband modulation and the width of the Si waveguide modulation, as shown in Fig. 3(d). In the calculation, Si waveguide width except for the width modulation region is assumed to be $w_{\text{Si}} = 0.8$ μm . The effective refractive index was calculated in optical-mode-profile simulations.

In this study, we decided to use the modulation depth of 7 nm to maximize the threshold gain difference. When the modulation width of the Si waveguide is set to be $\Delta w_{\text{Si}} = 80$ nm, the stopband modulation depth is $\Delta\lambda_b = 7$ nm. This is enough large to precisely control the stopband by modulating the Si waveguide width. To suppress the spatial hole burning effect, shallower modulation depth is preferable, as shown in Fig. 3(c), however, for easy to fabricate, we use 7-nm modulation depth. Please note that we can suppress spatial hole burning by reducing the optical confinement factor in active region, which can be controlled in III-V/Si supermode waveguide.

III. DEVICE FABRICATION

The device fabrication procedure is as follows. We use a silicon-on-insulator (SOI) substrate with a 220-nm-thick Si layer and a 2- μm -thick buried oxide (BOX) layer. First, Si waveguides containing the width-modulated waveguides are fabricated using a 220-nm-thick Si layer, which is then covered with a SiO_2 cladding film. For the wafer bonding process, the SiO_2 film is flattened by chemical polishing. After that, an InP substrate containing the InGaAsP-based six-layer MQWs is bonded to a SOI substrate by oxygen plasma assisted bonding. After removal of the InP substrate, the MQW layer is etched to form the core, and the InP is regrown to form the BH. The total III-V layer thickness is 230 nm. Zn thermal diffusion and Si ion implantation are used for p- and n-type doping, respectively. A uniform SiN grating without a phase shifter is formed on the top-surface of the III-V layer. The thickness of the SiN grating is 20 nm. The grating coupling coefficient is calculated to be 33 cm^{-1} . We use electron cyclotron resonance (ECR) plasma sputtering for low-temperature deposition of a smooth and thin SiN film with high uniformity [31]. After that, the entire InP layer is removed, except for the laser including the 100-nm-tip-width InP taper waveguides. Finally, metal electrodes and $3 \times 3\text{-}\mu\text{m}^2$ core-size SiO_x waveguides are fabricated.

IV. RESULTS AND DISCUSSION

A. Characteristics of Laser With Stopband-Modulated Cavity

We measured fabricated membrane III-V/Si BH DFB laser with 500- μm long active region [30]. We use an 840-nm wide Si waveguide with an 80-nm Si waveguide width modulation at the middle of the cavity, in accordance with the calculations described in Section II. The modulation length was 50 μm at the center. The fabricated lasers were performed under continuous-wave (CW) operations. In the experiment, single-mode high-numerical aperture fibers (HNAFs) were physically connected to the SiO_x waveguides for the device characterizations. Optical isolators were used for eliminating the reflections from the connectors and equipment, as shown in Fig. 4(a). The stage temperature was controlled by a Peltier cooler. Fig. 4(b) shows the output power versus injection current (I - L characteristic) at a stage temperature of 25 $^\circ\text{C}$. The current-voltage characteristic (I - V characteristic) is also shown. The vertical axis is the sum of the output power emitted from both facets. Also shown is the I - L characteristic, which was measured with a large-area photodetector (without HNAF) placed in front of the SiO_x waveguide facet. From these I - L characteristics, we estimated the fiber coupling loss to be about 2 dB, which is low compared with a conventional grating coupler. The threshold current and maximum fiber output power were 3 mA and 4 mW, respectively.

Fig. 5(a) shows the measured lasing spectrum under an injection current of 35 mA and a stage temperature of 25 $^\circ\text{C}$. We obtained single-mode lasing at a wavelength of 1552 nm with an SMSR of 55 dB. We calculated the emission spectrum on the basis of the transfer matrix model, as shown in Fig. 5(b). Good agreement with the experimental result was confirmed. The ripples on the longer wavelength side were suppressed compared

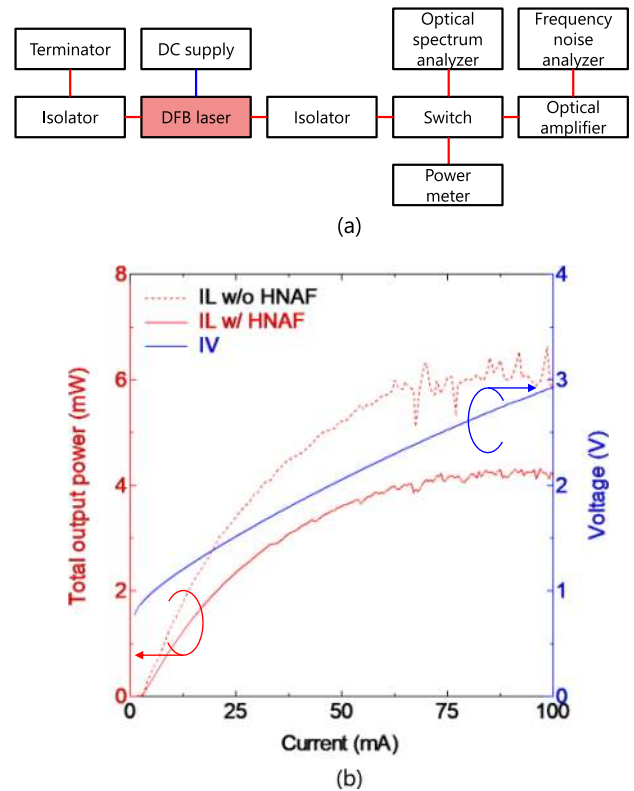


Fig. 4. (a) Experimental setup for measuring the laser characteristics. (b) Measured I - L characteristics at a stage temperature of 25 $^\circ\text{C}$ with and without HNAF.

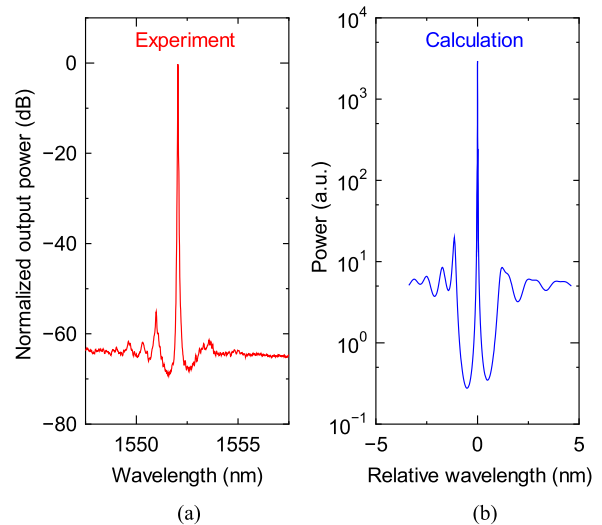


Fig. 5. (a) Measured lasing spectrum of laser with stopband-modulated cavity under an injection current of 35 mA and a stage temperature of 25 $^\circ\text{C}$ and (b) calculated emission spectrum.

with those on the shorter wavelength side. This is evidence that the stopband was modulated to the longer wavelength side.

We measured the frequency noise spectrum to estimate the Lorentzian linewidth of the fabricated laser. The experimental setup is also shown in Fig. 4(a). We use the commercial frequency noise analyzer (OEwaves, Inc., OE4000) to separate

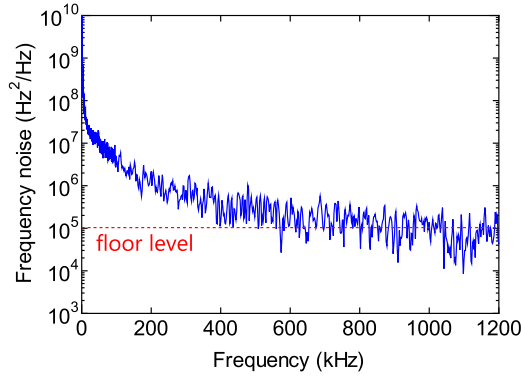


Fig. 6. Measured frequency noise spectrum under an injection current of 54 mA and a stage temperature of 25 °C.

the white noise from the technical noise such as vibration and power supply driving laser. From the white noise level, we can estimate the intrinsic Lorentzian linewidth of the laser by multiplying π with the white noise level. Fig. 6 shows the measured frequency noise spectrum under an injection current of 54 mA. We observed a white noise floor. By multiplying π with a floor noise level between 900 and 1200 kHz, the Lorentzian linewidth is estimated to be about 300 kHz.

From these results, it was demonstrated that the single-mode lasing can be obtained by using the uniform grating and width-modulated Si waveguide which is optically coupled with the III-V active layer. On the other hand, the maximum output power was limited to around 4 mW due to self-heating. The output power can be increased by extending the active region length since the thermal impedance can be reduced by extending that length, i.e., the bias current can be increased.

B. Extend of Cavity Length

In this above context, we also fabricated the membrane III-V/Si BH DFB laser with 1-mm long active region. In the long-cavity lasers, mitigating the optical power localization becomes more important for stable-single mode lasing. Therefore, we have to reduce the coupling coefficient compared with that of 500- μm long laser. In our device, coupling coefficient of the grating can be controlled by the optical confinement factor in SiN layer as shown in Fig. 2(a). Therefore, it can be controlled by the width of the Si waveguide. Fig. 7 shows the measured and calculated coupling coefficients as a function of Si waveguide width. As shown, the coupling coefficient is reduced by increasing the Si waveguide width. On the basis of these results, we use the Si waveguide with a width of 1 μm to reduce the coupling coefficient to about 27 cm^{-1} . We designed the modulation depth for maximizing the Δg_{th} to be $\Delta \lambda_{\text{b}} = 6 \text{ nm}$, corresponding to the Si waveguide modulation depth of 90 nm, where the base Si waveguide width is 1 μm .

We measured the output power versus the injection current for the 1-mm long laser. Fig. 8(a) shows the I - L characteristics for different stage temperatures. The I - V characteristic at a stage temperature of 25 °C is also shown. The threshold current and maximum output power were 5 mA and 17 mW, respectively, at

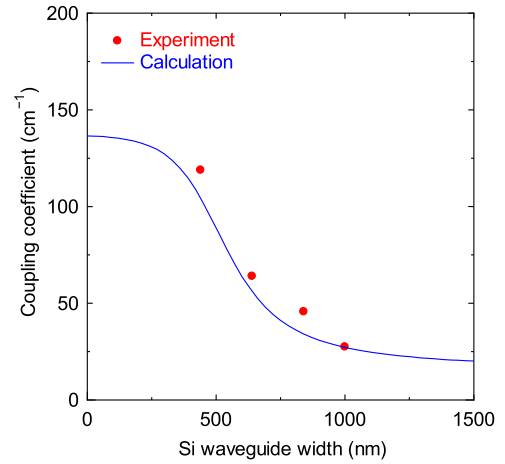


Fig. 7. Calculated and measured coupling coefficient for SiN grating versus Si waveguide width.

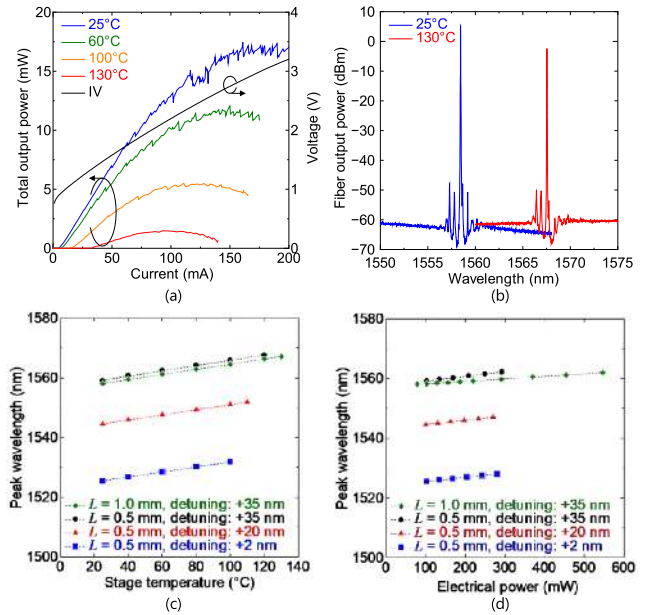


Fig. 8. (a) Measured I - L - v characteristics for different stage temperature. (b) Measured lasing spectra for stage temperature of 25 and 130 °C under the injection current of 70 mA. (c) Measured lasing wavelength shifts versus stage temperature (c) and injection electrical power (d).

a stage temperature of 25 °C. High-output power was obtained by making the cavity longer than the previous 0.5-mm long one. The fiber output power was 5 mW at a stage temperature of 100 °C. High-temperature operation up to 130 °C was obtained with 1-mW output power.

The optical spectrum at an injection current of 70 mA is shown in Fig. 8(b). We obtained single-mode lasing in the 1-mm long laser. Single-mode lasing was maintained while the peak wavelength shifted to a longer wavelength as the temperature increased.

C. Thermal Analysis

Finally, we confirmed the effect of lengthening of the active region on the thermal impedance. The lasing wavelength shifts

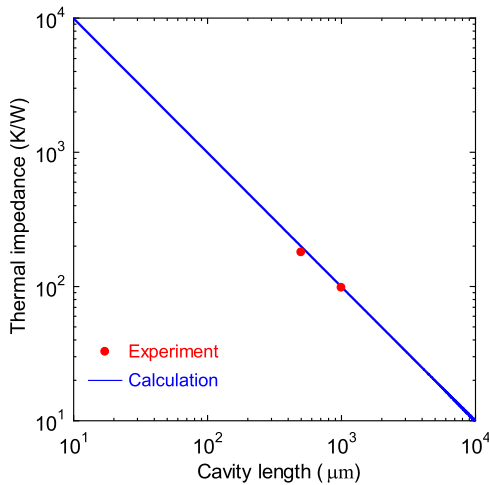


Fig. 9. Calculated and measured thermal impedance versus cavity length.

versus stage temperature and injection electrical power were measured in order to estimate the thermal impedance. Fig. 8(c) shows the measured lasing wavelength shift versus stage temperature for 0.5-mm-long and 1-mm-long lasers. Also shown are the lasing wavelength shifts for different wavelength detuning lasers with the 0.5-mm length. The devices all had almost the same shift. This is because the lasing wavelength depended on the effective index, which in turn depended on temperature, but not on the cavity length or detuning. Fig. 8(d) shows the measured lasing wavelength shift versus injection electrical power. Also shown are lasing wavelength shifts for different wavelength detuning lasers with a 0.5-mm length. The shifts are almost the same for different detuning lasers with the 0.5-mm length, but had different slopes for different length lasers. This indicates that the temperature increase by the injected electrical power is different for different length lasers. Fig. 9 shows the measured and calculated thermal impedances for the 0.5-mm-long and 1-mm-long lasers. In the calculation, a heat source was embedded in the p-InP region for simplicity. As shown, the thermal impedance was reduced by extending the active region. From these results, we conclude that the high-output power is the result of extending the active region and reducing the thermal impedance.

V. CONCLUSION

We developed a membrane BH DFB III-V/Si laser using a stopband-modulated cavity on Si substrate. The membrane III-V layer enables us to construct an optical supermode with a 220-nm-thick Si waveguide. The stopband modulation of the cavity is created by width modulation of the optically coupled Si waveguide and provides smoother and mitigated intensity localization compared with a cavity with a $\lambda/4$ -phase shift. The use of uniform grating and width-modulated Si waveguide has advantage for easy fabrication of single-mode laser. The laser is fabricated by a direct wafer bonding and epitaxial growth of membrane InP-based layers on a Si substrate. By using the 500- μ m-long DFB laser, we demonstrated that the single-mode

lasing can be obtained by using the uniform surface SiN grating and width-modulated Si waveguide. By extending the active region length to 1 mm, 17-mW fiber coupled output power is obtained. High-temperature operation up to 130 °C is also obtained with a 1-mW fiber output power. These results are obtained by using the Si waveguide with the 220-nm thickness. This development enables wafer-scale laser integration on a standard Si platform without having to change the thickness of the Si waveguide. The laser described here is promising for future high-capacity optical transmitters including lasers and MZMs on Si photonics platforms.

ACKNOWLEDGMENT

Part of this research were conducted as Commissioned Research, "R&D on optical PLL device for receiving and monitoring optical signals," of the National Institute of Information and Communications Technology (NICT), Japan.

REFERENCES

- [1] P. Dong, X. Liu, S. Chandraskhar, L. L. Buhl, R. Aroca, and Y.-K. Chen, "Monolithic silicon photonic integrated circuits for compact 100+GB/s coherent optical receivers and transmitters," *IEEE J. Sel. Topics Quantum Electron.*, vol. 20, no. 4, Jul./Aug. 2014, Art. no. 6100108.
- [2] T. Tsuchizawa *et al.*, "Microphotonics devices based on silicon micro-fabrication technology," *IEEE J. Sel. Quantum Electron.*, vol. 11, no. 1, pp. 232–240, Jan./Feb. 2005.
- [3] H. Fukuda, K. Yamada, T. Tsuchizawa, T. Watanabe, H. Shinjima, and S. Itabashi, "Silicon photonic circuit with polarization diversity," *Opt. Express*, vol. 16, no. 7, pp. 4872–4880, Mar. 2008.
- [4] C. R. Doerr, "Silicon photonic integration in telecommunications," *Frontiers Phys.*, vol. 3, pp. 1–16, Aug. 2015.
- [5] A. Abbasi *et al.*, "28 Gb/s direct modulation heterogeneously integrated C-band InP/SOI DFB laser," *Opt. Express*, vol. 23, no. 20, pp. 26479–26485, 2015.
- [6] T. Komljenovic, S. Srinivasan, E. Norberg, M. Davenport, G. Fish, and J. E. Bowers, "Widely tunable narrow-linewidth monolithically integrated external-cavity semiconductor lasers," *IEEE J. Sel. Topics Quantum Electron.* vol. 21, no. 6, Nov./Dec. 2015, Art. no. 1501909.
- [7] C. T. Santis, S. T. Steger, Y. Vilenchik, A. Vasilyev, and A. Yariv, "High-coherence semiconductor lasers based on integral high-Q resonators in hybrid Si/III-V platform," *Proc. Nat. Acad. Sci. USA*, vol. 111, pp. 2879–2884, 2014.
- [8] C. T. Santis, Y. Vilenchik, N. Satyan, G. Rakuljic, and A. Yariv, "Quantum control of phase fluctuations in semiconductor lasers," *Proc. Nat. Acad. Sci. USA*, vol. 115, pp. 7896–7904, 2018.
- [9] P. Dong *et al.*, "Novel integration technique for silicon/III-V hybrid laser," *Opt. Express*, vol. 22, no. 22, pp. 26854–26861, 2014.
- [10] B. Jang *et al.*, "A hybrid silicon evanescent quantum dot laser," *Appl. Phys. Express*, vol. 9, 2016, Art. no. 092102.
- [11] T. Ferrotti *et al.*, "Co-integrated 1.3 μ m hybrid III-V/silicon tunable laser and silicon Mach-Zehnder modulator operating at 25 Gb/s," *Opt. Express* vol. 24, no. 26, pp. 30379–30401, 2016.
- [12] M. Tran, D. Huang, T. Komljenovic, J. Peters, A. Malik, and J. Bowers, "Ultra-low-loss silicon waveguides for heterogeneously integrated silicon/III-V photonics," *Appl. Sci.*, vol. 8, no. 7, p. 1139, 2018.
- [13] M. Tran, D. Huang, and J. Bowers, "Tutorial on narrow linewidth tunable semiconductor lasers using Si/III-V heterogeneous integration," *APL Photon.*, vol. 4, 2019, Art. no. 111101.
- [14] D. Huang *et al.*, "High-power sub-kHz linewidth lasers fully integrated on silicon," *Optica*, vol. 6, no. 6, pp. 745–752, 2019.
- [15] M. Tran, D. Huang, J. Guo, T. Komljenovic, P. Morton, and J. Bowers, "Ring-resonator based widely-tunable narrow-linewidth Si-InP integrated lasers," *IEEE J. Sel. Top. Quantum Electron.* vol. 26, no. 2, Mar./Apr. 2020, Art. no. 1500514.
- [16] S. Matsuo, T. Fujii, K. Hasebe, K. Takeda, T. Sato, and T. Kakitsuka, "Directly modulated buried heterostructure DFB laser on SiO₂/Si substrate fabricated by regrowth of InP using bonded active layer," *Opt. Express*, vol. 22, no. 10, pp. 12139–12147, 2014.

- [17] S. Matsuo, T. Fujii, K. Hasebe, K. Takeda, T. Sato, and T. Kakitsuka, "Directly modulated DFB laser on SiO₂/Si substrate for datacenter networks," *IEEE J. Lightw. Technol.*, vol. 33, no. 6, pp. 1217–1222, Mar. 2015.
- [18] H. Nishi *et al.*, "Membrane distributed-reflector laser integrated with SiO_x-based spot-size converter on Si substrate," *Opt. Express*, vol. 24, no. 16, pp. 18346–18352, 2016.
- [19] T. Fujii *et al.*, "Heterogeneously integrated membrane lasers on Si substrate for low operating energy optical links," *IEEE J. Sel. Top. Quantum Electron.*, vol. 24, no. 1, Jan./Feb. 2018, Art. no. 1500408.
- [20] E. Kanno *et al.*, "Twin-mirror membrane distributed-reflector lasers using 20- μ m-long active region on Si substrate," *Opt. Express*, vol. 26, no. 2, pp. 1268–1277, 2018.
- [21] T. Aihara *et al.*, "Lateral current injection membrane buried heterostructure lasers integrated on 200-nm-thick Si waveguide," in *Proc. Opt. Fiber Commun. Conf. Expo.*, 2018, paper W3F4.
- [22] Y. Akahane, T. Asano, B.-S. Song, and S. Noda, "High-Q photonic nanocavity in a two-dimensional photonic crystal," *Nature*, vol. 425, pp. 944–947, 2003.
- [23] B.-S. Song, S. Noda, T. Asano, and Y. Akahane, "Ultra-high-Q photonic double-heterostructure nanocavity," *Nature Mater.*, vol. 4, pp. 207–210, 2005.
- [24] M. Notomi, "Manipulating light with strongly modulated photonic crystals," *Rep. Prog. Phys.*, vol. 73, no. 9, pp. 1–57, 2010.
- [25] E. Kuramochi, H. Taniyasu, T. Tanabe, K. Kawasaki, Y.-G. Roh, and M. Notomi, "Ultra-high-Q one-dimensional photonic crystal nanocavities with modulated mode-gap barrier on SiO₂ claddings and on air claddings," *Opt. Express*, vol. 18, no. 15, pp. 15859–15869, 2010.
- [26] H. Soda, Y. Kotaki, H. Sudo, H. Ishikawa, S. Yamakoshi, and H. Imai, "Stability in single longitudinal mode operation in GaInAsP/InP phase-adjusted DFB lasers," *IEEE J. Sel. Topics Quantum Electron.* vol. 23, no. 6, pp. 804–814, Jun. 1987.
- [27] M. Okai, T. Tsuchiya, K. Uomi, N. Chinone, and T. Harada, "Corrugation-pitch modulated MQW-DFB lasers with narrow spectral linewidth," *IEEE J. Sel. Topics Quantum Electron.*, vol. 27, no. 6, pp. 1764–1772, Jun. 1991.
- [28] S. Ogita, Y. Kotaki, M. Matsuda, Y. Kuwahara, and H. Ishikawa, "Long-cavity multiple-phase-shift distributed feedback laser diode for linewidth narrowing," *IEEE J. Lightw. Technol.*, vol. 8, no. 10, pp. 1596–1604, Oct. 1990.
- [29] H. Ishii, K. Kasaya, and H. Oohashi, "Spectral linewidth reduction in sidely wavelength tunable DFB laser array," *IEEE J. Sel. Topics Quantum Electron.*, vol. 15, no. 3, pp. 514–520, May/Jun. 2009.
- [30] T. Aihara, T. Hiraki, T. Fujii, K. Takeda, T. Tsuchizawa, T. Kakitsuka, and S. Matsuo, "Membrane III-V/Si DFB laser with width modulated silicon waveguide for narrowing linewidth," in *Proc. 45th Eur. Conf. Opt. Commun.*, 2019, paper Tu.2.D.5.
- [31] T. Amazawa, T. Ono, M. Shimada, S. Matsuo, and H. Oikawa, "Ultrathin oxide films deposited using electron cyclotron resonance sputter," *J. Vac. Sci. Technol. B*, vol. 17, no. 5, pp. 2222–2225, 1999.

Takuma Aihara (Member, IEEE) was born in Akita, Japan in 1987. He received the B.E., M.E., and Ph.D. degrees in electrical and electronic information engineering from the Toyohashi University of Technology, Aichi, Japan, in 2010, 2012, and 2015, respectively.

He joined NTT Device Technology Laboratories in 2015. He has been doing research on the III–V semiconductor lasers on Si photonic integrated circuits.

Dr. Aihara is a member of the Japanese Society of Applied Physics.

Tatsuro Hiraki (Member, IEEE) received the B.E., M.E., and Ph.D. degrees in engineering from Tohoku University, Sendai, Japan, in 2009, 2011, and 2017, respectively. In 2011, he joined NTT Microsystem Integration Laboratories, Nippon Telegraph and Telephone Corporation, Kanagawa, Japan. His current research interests include heterogeneously integrated III–V semiconductor Mach-Zehnder modulators, optical amplifiers, and laser diodes on Si photonics circuits. He is a member of the Institute of Electronics, Information and Communication Engineers and the Japan Society of Applied Physics.

Takuro Fujii (Member, IEEE) was born in Kyoto, Japan in 1986. He received the B.E. and M.E. degrees in system design engineering from Keio University, Kanagawa, Japan, in 2010 and 2012, respectively.

He joined NTT Photonics Laboratories in 2012. He has been doing research on MOVPE growth of III–V semiconductors and the development of III–V semiconductor lasers on Si for photonic integrated circuits.

Mr. Fujii is a member of the Institute of Electronics, Information and Communication Engineers and the Japanese Society of Applied Physics (JSAP). He received the Young Scientist Presentation Award from the JSAP in 2014.

Koji Takeda (Senior Member, IEEE) received the B.S., M.S., and Ph.D. degrees in electronics engineering from the University of Tokyo, Tokyo, Japan, in 2005, 2007, and 2010, respectively.

From 2008 to 2010, he received research fellowship for young scientists from the Japan Society for the Promotion of Science. In 2010, he joined NTT Photonics Laboratories. In 2018, he was also with IHP microelectronics GmbH as a Visiting Researcher. His current research interests include ultralow-power optical interconnect, photonic integrated circuit, and photonic crystal lasers.

He is a member of the IEICE and the JSAP. He is the recipient of the Best Student Paper Award from the IEEE Photonics Society in 2009, the Outstanding Student Presentation Award from JSAP in 2010, and the Best Paper Award from the IEICE in 2012.

Takaaki Kakitsuka (Member, IEEE) was born in Kumamoto, Japan, in 1971. He received the B.S. and M.S. degrees in physics and the Dr. Eng. degree from Kyushu University, Fukuoka, Japan, in 1994, 1996, and 2012, respectively.

In 1996, he joined NTT Opto-Electronics Laboratories, Nippon Telegraph and Telephone Corporation, Kanagawa, Japan. He was involved in the research on semiconductor lasers and optical integrated devices at NTT Corporation from 1996 to 2019. In 2019, he became an Associate Professor with the Graduate School of Information, Production and Systems, Waseda University, Fukuoka. He has been involved in the research on semiconductor lasers and their information communication system applications.

Dr. Kakitsuka is a member of the IEICE, JSAP, and the Physical Society of Japan.

Tai Tsuchizawa, biography not available at the time of publication.

Shinji Matsuo (Fellow, IEEE) received the B.E. and M.E. degrees in electrical engineering from Hiroshima University, Hiroshima, Japan, in 1986 and 1988, and the Ph.D. degree in electronics and applied physics from Tokyo Institute of Technology, Tokyo, Japan, in 2008.

In 1988, he joined NTT Opto-electronics Laboratories, Atsugi, where he was engaged in the research on photonic functional devices using MQW-pin modulators and VCSELs. In 1997, he researched optical networks using WDM technologies with NTT Network Innovation Laboratories, Yokosuka, Japan. Since 2000, he has been researching InP-based photonic integrated circuits with NTT Photonics Laboratories and NTT Device Technology Laboratories, Atsugi.

Dr. Matsuo is a member of Japan Society of Applied Physics and the Institute of Electronics, Information, Communication Engineers of Japan.